

Review

Phase Conversions in Neutron Stars: Implications for Stellar Stability and Gravitational Wave Astrophysics

Germán Lugones ^{1,*}  and Ana Gabriela Grunfeld ^{2,3} 

¹ Centro de Ciências Naturais e Humanas, Universidade Federal do ABC, Avenida dos Estados 5001—Bangú, Santo André CEP 09210-580, SP, Brazil

² Departamento de Física, Comisión Nacional de Energía Atómica, Av. Libertador 8250, Buenos Aires 1429, Argentina; grunfeld@tandar.cnea.gov.ar

³ CONICET, Godoy Cruz, Buenos Aires 2290, Argentina

* Correspondence: german.lugones@ufabc.edu.br

Abstract: We review the properties of hybrid stars with a quark matter core and a hadronic mantle, focusing on the role of key micro-physical properties such as the quark/hadron surface and curvature tensions and the conversion speed at the interface between both phases. We summarize the results of works that have determined the surface and curvature tensions from microscopic calculations. If these quantities are large enough, mixed phases are energetically suppressed and the quark core would be separated from the hadronic mantle by a sharp interface. If the conversion speed at the interface is slow, a new class of dynamically stable hybrid objects is possible. Densities tens of times larger than the nuclear saturation density can be attained at the center of these objects. We discuss possible formation mechanisms for the new class of hybrid stars and smoking guns for their observational identification.

Keywords: neutron star; equation of state; surface tension of dense matter; gravitational waves; stellar stability



Citation: Lugones, G.; Grunfeld, A.G. Phase Conversions in Neutron Stars: Implications for Stellar Stability and Gravitational Wave Astrophysics. *Universe* **2021**, *7*, 493. <https://doi.org/10.3390/universe7120493>

Academic Editors: Ignazio Bombaci and Rosa Poggiani

Received: 3 November 2021

Accepted: 9 December 2021

Published: 13 December 2021

Publisher's Note: MDPI stays neutral with regard to jurisdictional claims in published maps and institutional affiliations.



Copyright: © 2021 by the authors. Licensee MDPI, Basel, Switzerland. This article is an open access article distributed under the terms and conditions of the Creative Commons Attribution (CC BY) license (<https://creativecommons.org/licenses/by/4.0/>).

1. Introduction

A longstanding unsolved problem in neutron star (NS) physics is whether deconfined quark matter can be present at their cores, which would imply the existence of the so-called hybrid stars, composed by a quark matter core and a hadronic mantle. At present, the state of matter in the crust and in the inner core of NSs (up to $\sim 1 - 2n_0$, being $n_0 = 0.16 \text{ fm}^{-3}$ the nuclear saturation density) is reasonably well understood and constrained by theory and experiments. However, the behavior of matter occupying the inner core, where the density exceeds $2n_0$, still faces theoretical challenges and can only be constrained by astrophysical observations.

Fortunately, in recent years, many substantial advances have been made in the determination of some key properties of NSs that can be directly related to their internal composition. In particular, a set of pulsars with masses around $\sim 2 M_\odot$ have been discovered (PSR J1614-2230 [1], PSR J0348+0432 [2], PSR J0740+6620 [3], and PSR J2215-5135 [4]), which require that any model for the equation of state of dense matter must be able to produce stellar configurations with at least two solar masses. Additionally, joint mass-radius measurements with increasing precision are available from the Neutron Star Interior Composition Explorer (NICER) which is the first mission specifically designed for the study of NSs. Using the pulse profile modeling technique that exploits hotspots on the NS surface, the mass and radius of the millisecond-pulsars PSR J0030+0451 [5,6] and PSR J0740+6620 [7,8] has been measured with great precision. Interestingly, the inferred radius of PSR J0740+6620 (with $\sim 2 M_\odot$) is very similar to that of PSR J0030+0451 (with $\sim 1.4 M_\odot$), even though they have very different masses [7,8].

New limits on the EOS were posed recently by the LIGO/Virgo detection of gravitational-waves (GWs) coming from the NS-NS merger event GW170817 [9–13]. Assuming that both NSs are described by the same EOS and have spins within the range observed in Galactic binary NSs, the dimensionless tidal deformability $\Lambda_{1.4}$ of a $1.4 M_{\odot}$ NS was found to be in the range 70–580 at the 90% level [14]. The event was also accompanied by a multi-wavelength electromagnetic counterpart, from γ -rays to radio. In addition, the fact that the postmerger remnant of GW170817 did not suffer a prompt collapse was used to constrain the maximum gravitational mass of a nonrotating NS ($M_{\text{max}} \approx 2.3 M_{\odot}$) [15]. Later, the LIGO Livingston detector observed the event GW190425, a compact binary coalescence with total mass $\sim 3.4 M_{\odot}$ [16]. This was the first confirmed GW detection based on data from a single observatory and no electromagnetic counterpart was found. If interpreted as a double NS merger, the total gravitational mass is substantially larger than that of binary systems identified in the Galaxy. This raises the possibility of GW190425 being a NS-black hole (BH) binary merger [17,18]. Next, the LIGO/ Virgo Collaboration announced the discovery of a gravitational wave binary, GW190814 [19] from which no electromagnetic counterpart was identified. One component of this binary is a $23 M_{\odot}$ BH while the other is a $2.6 M_{\odot}$ object. The mass of the secondary leaves the nature of this component ambiguous: while the Bayesian analysis of Reference [20] favors the scenario that the event was a binary BH merger, the secondary of GW190814 can also be interpreted as a massive rapidly-rotating NS with exotic degrees of freedom [21] or a color-flavor-locked strange quark star [22]. Finally, the LIGO/Virgo collaboration announced the discovery of GW200105 and GW200115 [23]. The first binary, GW200105, was later reported as a marginal candidate [24]. The second one, GW200115, has a $5.7 M_{\odot}$ BH and a $1.5 M_{\odot}$ NS. No electromagnetic counterparts were detected for either system. More recently, the LIGO/Virgo O3b run reported new events involving NSs, cf. GW191219 (NS-BH) and GW200210 (NS-BH or BH-BH) [24].

On the theoretical front, a reliable description of the equation of state of matter above $\sim 1 - 2n_0$ still faces many difficulties that are bypassed by using phenomenological models that match experimental data at low densities and perturbative QCD at asymptotically large ones. Within such an approach, many internal compositions are possible that agree with all present theoretical and empirical requirements. Among them, hybrid stars have attracted much attention because quantum chromodynamics predicts that at sufficiently high energy densities, hadronic matter undergoes a deconfinement transition to a phase of quarks and gluons. There are still many open questions related to hybrid stars, probably the most important one being whether the central densities of these objects are large enough to allow for deconfined quark matter. In the present review we assume as a working hypothesis that deconfined matter do exist at NS cores and explore the role of several microphysical properties of dense matter on the internal structure of these objects. In particular, we pay special attention to the behavior of the quark hadron interface (surface, tension, curvature energy, speed of conversion reactions) and their consequences on stellar structure and stability.

This review is organized as follows. In Section 2 we discuss the relevance of dense matter surface (and curvature) tension for the quark–hadron interface in hybrid stars. In particular, it is known that the surface tension determines the formation (or not) of the so called quark–hadron mixed phase, made of lumps of one phase embedded in a background of the other one. We summarize the results of works that have determined the surface tension from microscopic calculations and explore the implications for NS physics. In Section 3, we discuss recent results on the dynamic stability of hybrid stars. It is shown that the speed of hadron \leftrightarrow quark conversion reactions that may occur when the interface of a hybrid star is perturbed has a determinant impact on the dynamic stability of the hybrid star. If conversions have a sufficiently large timescale, a new branch of stable hybrid stars is possible, with several physical and astrophysical consequences. Unfortunately, the conversion timescale is unknown at present, but we provide some arguments and model dependent results that indicate that it would be slow. In Section 4 we examine

some possible mechanisms for the formation of the new class of hybrid stars in realistic astrophysical situations. In Section 5 we identify some signatures that can help in their observational identification, in particular by means of the detection of gravitational waves. We finish with some conclusions in Section 6.

2. The Nature of the Quark Hadron Interface: Sharp or Mixed?

A comprehensive study of the surface tension σ of deconfined quark matter is of greatest importance for a better understanding of the internal composition of NSs [25–28] as well as for determining the nucleation rate and the associated critical size of the nucleated drops [29,30] at the deep core of NSs. In addition, surface tension affects decisively the properties of the most external layers of a strange star which may fragment into a charge-separated mixture, involving positively-charged strangelets immersed in a negatively charged sea of electrons, presumably forming a crystalline solid crust [31]. This would happen below a critical surface tension which is typically of the order of $\sim 10 \text{ MeV}/\text{fm}^2$ [32,33]. The surface tension is also crucial for the quark–hadron interface of a hybrid star, which might form a mixed phase for values of σ below some tens of MeV/fm^2 [34–37]. Here we will focus on the hybrid star case.

In the core of compact stars, when the density exceeds the nuclear saturation density, a deconfinement transition from hadronic to quark matter might occur. Usually, a hybrid description of strongly interacting matter is used, in which a hadronic model which is reliable at low densities is extrapolated to higher ones and matched with a quark model. This situation is qualitatively depicted in the right panel of Figure 1, where the Gibbs free energy per baryon G/n_B of both phases intersect at a transition pressure p_{tr} , being the energetically preferred phase the one with lower G/n_B . Then, the quark–hadron transition is of the first order by construction and the resulting equation of state predicts a stellar configuration that contains a sharp interface separating a pure quark matter core from a purely hadronic mantle.

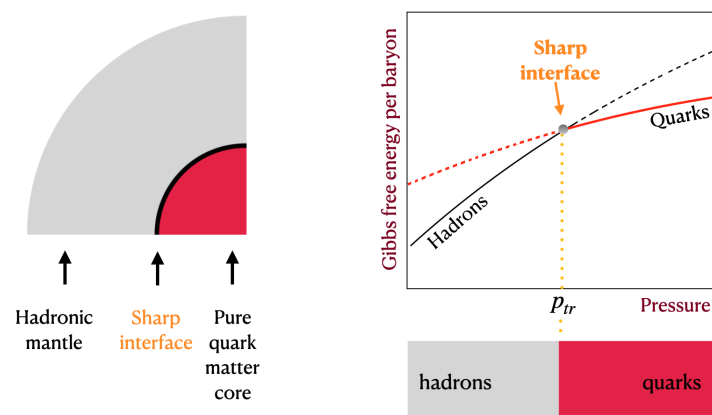


Figure 1. Sketch of the interior of a hybrid star and schematic representation of the Gibbs free energy per baryon in the case of a sharp interface.

The previous scenario presumes that the electric charge is locally neutral. However, there is a change in G/n_B when global (instead of local) electric charge neutrality is allowed, which is due to the formation of electrically charged geometric structures that have a surface, curvature, and Coulomb energy cost. Calculations show that in general the surface contribution dominates over the others. As a consequence (see right panel of Figure 2), there is a decrease of G/n_B if the surface tension is low enough (orange line) or an increase of G/n_B in the opposite case (blue line). The value of σ for which the globally neutral and the locally neutral phases have the same G/n_B at p_{tr} is known as critical surface tension σ_{crit} . If the surface tension exceeds σ_{crit} (which is of the order of tens MeV/fm^2 [34–37]) the energy cost of global charge neutrality is too high and a sharp interface is expected as described in Figure 1. On the contrary, if the surface tension is

smaller than σ_{crit} , a mixed phase where lumps of one phase are embedded in a background of the other one is expected (see Figure 2). Depending on the models and on the value of σ , the mixed phase would include different geometrical structures (droplets, rods, slabs, tubes, and bubbles [38–40]) present over a wide density range of the stellar core.

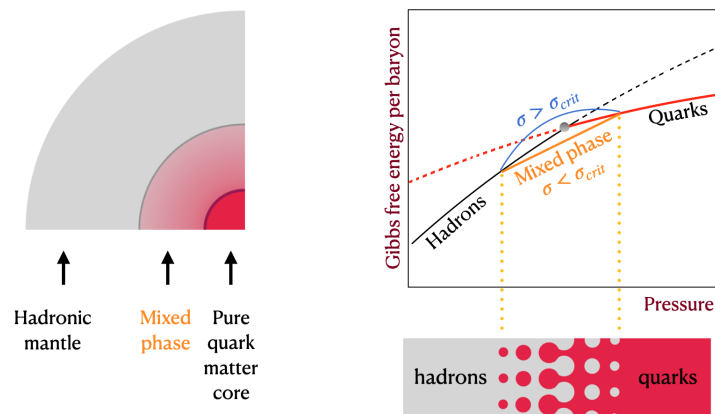


Figure 2. Same as in the previous figure but for a mixed interface.

Several works in the literature have used the quark matter surface tension as a free parameter to describe the possible structure of mixed phases and to evaluate under which conditions it would be favored over a sharp quark–hadron interface (see e.g., [32,34,38,41–44] and references therein). However, there are fewer works that have determined the surface tension σ and the curvature tension γ from microscopic calculations. In Table 1 we summarize the results obtained for σ within different effective equations of state and using different techniques for the microscopic calculation. For comparison, we include also lattice QCD results in the vanishing baryon number density and high temperature regime. The results span a wide range of values. Assuming σ_{crit} of some tens of MeV/fm², some calculations suggest the existence of a mixed phase while others indicate that a sharp interface would be favored. On the other hand, the curvature tension γ has been less explored than σ . Within the Multiple Reflection Expansion (MRE) formalism [45,46], light quarks tend to have a minor contribution to σ but have a dominant role in γ . However, both effects, surface and curvature, are relevant in principle for massive enough species, like the *s* quark. Since the grand thermodynamic potential is $\Omega = -PV + \sigma S + \gamma C$ (being *V*, *S* and *C* the volume, surface, and curvature of a quark lump), the quantity $\gamma C / (\sigma S)$ encodes the relative influence of the surface and the curvature contribution. For spherical drops the ratio is $2\gamma / (R\sigma)$, showing that the curvature may be relevant and even dominant for small enough droplets [33,47].

The surface tension σ_h of hadronic matter is roughly below 1 MeV/fm² in the crust [34,48–50]. If the same order of magnitude is assumed for typical core densities, it turns out that the nuclear matter contribution would be much smaller than the quark matter one, as seen in Table 1. With that assumption, the existence of the quark–hadron mixed phase would be determined primarily by the surface tension of quark matter.

Table 1. Summary of microscopic calculations of the surface tension. See the works listed in the second column and references therein.

Equation of State + Method	Reference	σ [MeV/fm ²]	Remarks
Lattice QCD	[51–54]	5–20	vanishing baryon chemical potential, finite T
MIT bag model + Multiple Reflection Expansion	[33,55–57]	<25	for $n_B < 10n_0$, finite T , magnetic field, ν -trapping
Nambu-Jona-Lasinio model + geometric approach/thin wall	[26,58,59]	<25–30 for $B = 0$, ~ 70 for $B = 15m_\pi^2$	finite T , with/without magnetic field B
Linear sigma model + geometric approach/thin wall	[26,28,60]	<15 for $B = 0$, <60 for $B < 20m_\pi^2$	zero/finite T , with/without magnetic field B
Polyakov-quark-meson model + thin wall	[61]	<30	finite T
Dyson-Schwinger equation + thin wall approximation	[62]	<40	finite T
Nucleon-meson model + domain wall or bubble profiles	[63]	<15	finite T , model does not contain explicit quark degrees of freedom
Equivparticle model + Multiple Reflection Expansion/finite box	[64]	3–10	$T = 0$
Quasiparticle model + Multiple Reflection Expansion	[27]	30–70	$T = 0$
Nambu-Jona-Lasinio model + Multiple Reflection Expansion	[65]	145–165	finite T
vector MIT bag model + Multiple Reflection Expansion	[47]	5–300	for $n_B < 10n_0$, finite T , ν -trapping, huge vector contribution to σ

3. The Speed of Phase Conversions at the Quark-Hadron Interface and Its Role in Stellar Stability

In this section we will analyze the dynamic stability of hybrid stars. As shown by Chandrasekhar [66], stability can be assessed by inspecting the response of equilibrium configurations to small radial disturbances. When a dynamically *stable* star is perturbed, fluid elements along the interior oscillate around their equilibrium positions, compressing and expanding periodically. Instead, in a dynamically *unstable* star, small perturbations grow without limit, leading to the collapse or disruption of the object. The formalism of small radial perturbations of spherically symmetric stars shows that stellar configurations are stable if the frequency ω_0 of the fundamental mode verifies $\omega_0^2 \geq 0$ and unstable if $\omega_0^2 < 0$ [66].

For cold compact stars in chemical equilibrium (cold catalyzed matter) and without density discontinuities, it can be shown that changes of stability ($\omega_0 = 0$) occur at maxima or minima in the $M - \epsilon_c$ diagram, being M the stellar mass and ϵ_c the energy density at the stellar center [67]. Thus, the following much simpler *static* stability criterion holds [67]:

$$\frac{\partial M}{\partial \epsilon_c} < 0 \quad \Rightarrow \quad \omega_0^2 < 0 \quad (\text{unstable star}), \tag{1}$$

$$\frac{\partial M}{\partial \epsilon_c} > 0 \quad \Leftarrow \quad \omega_0^2 \geq 0 \quad (\text{stable star}). \tag{2}$$

For cold catalyzed hybrid stars with mixed phases, the latter static conditions remain valid, because the density varies continuously all along the stellar interior. However, in the case of hybrid stars with sharp discontinuities, Chandrasekhar’s analysis is not straightforward, since radial perturbations may induce the phase conversion of fluid elements in the neighborhood of the interface. Indeed, it has been shown that the conversion speed between quarks and hadrons at a sharp interface may produce significant changes

in the dynamic stability of the object [68–74]. In the following subsection we will describe the conditions under which the standard Equations (1) and (2) are not valid for hybrid stars with sharp interfaces.

3.1. Extended Dynamical Stability

When analyzing the response of hybrid stars to small radial perturbations, caution must be taken with fluid elements close to the quark–hadron interface, because, as the fluid oscillates, their pressures take values above and below the phase transition pressure p_{tr} . There are two essentially different behaviors depending on the speed of the quark–hadron conversion mechanism. If the conversion timescale is much shorter than the oscillation period (rapid conversions), fluid elements change periodically from one phase to the other as the pressure oscillates around p_{tr} . On the other hand, if the conversion timescale is much larger than the oscillation period (slow conversions), the motion around the interface involves only the stretch and squash of volume elements without any phase transformation (see Figure 3). Calculations show that ω_0 is of the order of magnitude of $\sim 1\text{--}100$ kHz for essentially all known dense matter EOSs [75–79]. Therefore, oscillations would be rapid or slow depending on whether the conversion timescale is smaller or larger than $\sim 0.01\text{--}1$ ms.

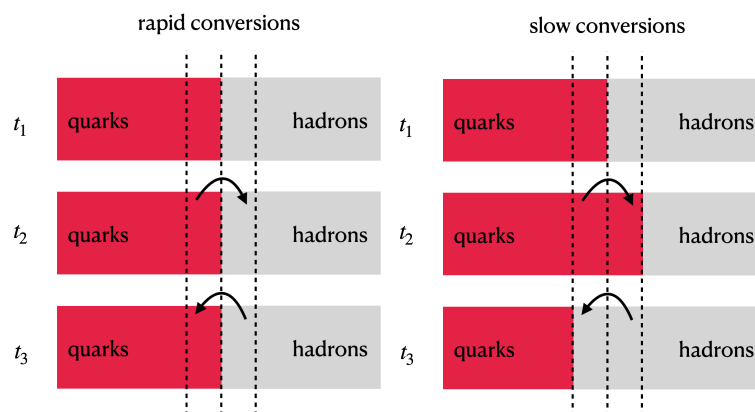


Figure 3. Neighborhood of the quark–hadron interface at three different times $t_1 < t_2 < t_3$ for rapid conversions (left) and slow conversions (right). At t_1 the interface is unperturbed; at t_2 a perturbation shifts a quark fluid element radially to a region with pressure below p_{tr} . If the conversion timescale is smaller than the oscillation period, the fluid element converts into hadrons before returning to the region with $p > p_{tr}$ at time t_3 . If the conversion timescale is larger than the oscillation period, the fluid element has not enough time for converting into hadrons before returning to the region with $p > p_{tr}$ at time t_3 .

In spite of the complexity of the phase changing mechanism, the fact that the phase splitting surface stays at the same place if conversions are rapid, and oscillates with the same period of perturbations if conversions are slow (see Figure 3), implies that the nature of the conversion can be encoded into simple junction conditions on the radial fluid displacement ζ and the corresponding Lagrangian perturbation of the pressure Δp at the interface [69].

For slow conversions, the resulting condition is that the jump of ζ and Δp across the interface should always be null [69]:

$$[\zeta]_{\pm}^{\pm} \equiv \zeta^+ - \zeta^- = 0, \quad [\Delta p]_{\pm}^{\pm} \equiv \Delta p^+ - \Delta p^- = 0, \tag{3}$$

where $[x]_{\pm}^{\pm} \equiv x^+ - x^-$ is the jump of a quantity x across the interface, being x^+ the value of x just above the interface (i.e., at the hadronic side) and x^- the value just below it (i.e., at the quark side).

For rapid phase transitions it was found that [69]:

$$[\zeta^r]_{-}^{+} = \Delta p \left[\frac{1}{p'_0} \right]_{-}^{+}, \quad [\Delta p]_{-}^{+} = 0, \quad (4)$$

where $p'_0 \equiv dp_0/dr$ is the gradient of the background pressure at the interface.

Using the junction conditions of Equations (3) and (4), the dynamic stability of hybrid stars with rapid and slow interface conversions has been analyzed in several recent works [68–74,80]. If conversions at the interface are rapid, calculations show that Equations (1) and (2) remain valid, and changes of stellar stability occur only at maxima or minima in the mass versus radius or the mass versus central energy density diagram. This is easy to understand physically because, in the case of rapid conversions, fluid elements around the interface are able to attain chemical equilibrium very fast. This means that the hypothesis of cold catalyzed matter necessary for the fulfillment of Equations (1) and (2) is always verified. On the contrary, changes of stability do not occur necessarily at critical points if the interface conversions are slow. Indeed, calculations show that ω_0 can be a real number (indicating stability) even if $\partial M/\partial \epsilon_c < 0$ [68–74]. Thus, in the case of slow conversions, many configurations that were believed to be radially unstable are in fact radially stable under small perturbations. These configurations have been called *slow-stable hybrid stars* in Reference [74].

Some practical consequences of the behavior described above are shown in the schematic curves of Figures 4 and 5, which were constructed based on the results of References [68–74]. In Figure 4, it is assumed that the quark–hadron interface occurs at high densities. The typical result that emerges from calculations is shown in the right panel where a branch of *slow-stable hybrid stars* appears for central densities higher than the one of the object with maximum mass. The baryon number density at the center of these hypothetical objects can be as high as some tens of n_0 (in fact, models with up to 66 n_0 at the center of the last stable object were obtained in Reference [74]). Such high central densities were obtained in Reference [74] for density jumps at the quark–hadron interface of 1000–3000 MeV/fm³. In Figure 5, it is assumed that the quark–hadron interface occurs at low densities. If interface reactions are rapid, the totally stable hybrid branch may be connected or disconnected from the hadronic one. In the left panel of Figure 5, we show a situation where the hybrid branch is disconnected from the hadronic one by a short segment of unstable models that starts at the onset of a quark matter core and ends at the local minimum of the curve’s valley. However, if interface conversions are slow, objects in that short segment become stable ($\omega_0^2 \geq 0$), and disconnected branches become connected (see right panel of Figure 5). For these models there exist low mass triplets of stars with the same gravitational mass but different radii in the vicinity of the valley. Models like the one shown in the right panel of Figure 4 can be obtained very easily provided one adopts a sufficiently stiff hadronic matter equation of state. However, models like the one presented in the right panel of Figure 5 require some fine tuning of the equations of state to fulfill the requirement of a maximum mass above $\sim 2 M_{\odot}$. Other geometries of the mass-radius relation are possible in principle, but the most common one involving *slow-stable hybrid stars* is by far the one shown in the right panel of Figure 4.

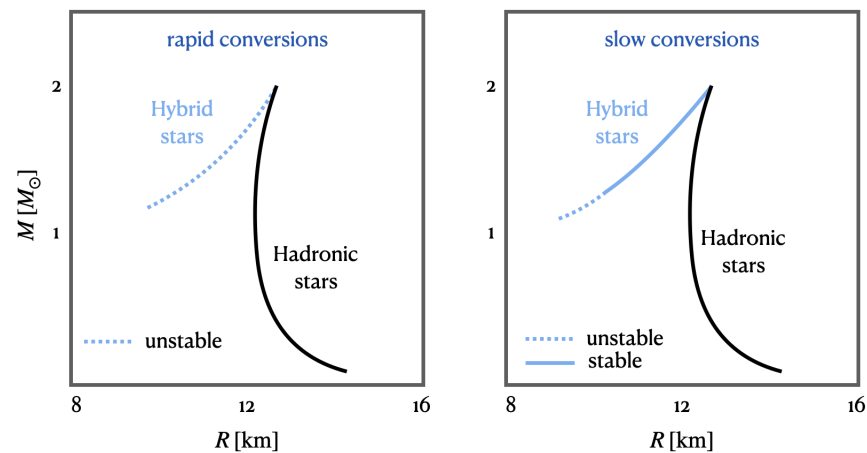


Figure 4. Mass–radius relationships for hybrid stars in the case of rapid and slow conversions. The curves represent qualitatively results that have been obtained with several combinations of realistic hadronic and quark equations of state [68–74,80]. In this figure, it is assumed that the hadron–quark interface occurs at high densities, thus, purely hadronic stars are possible up to $\sim 2M_{\odot}$. When rapid conversions are assumed (left panel), calculations show that the fundamental oscillation frequency of hybrid stars verifies $\omega_0^2 < 0$, indicating that hybrid configurations (dashed lines) are dynamically unstable. Considering the same equations of state, but assuming that interface conversions are slow (right panel), it is found that many hybrid stars have $\omega_0^2 > 0$ in spite of being in a branch with $\partial M/\partial \epsilon_c < 0$ (*slow-stable hybrid stars*). They are represented by thick lines in the right panel.

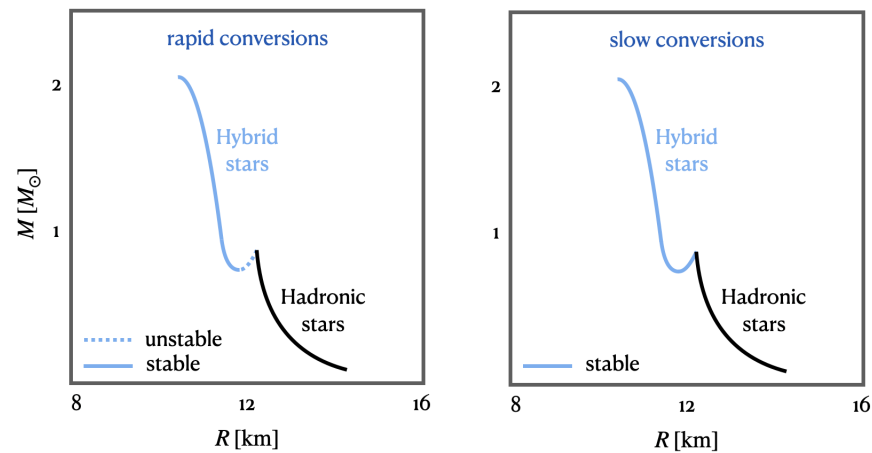


Figure 5. Same as in the previous figure but for a scenario where the hadron–quark interface occurs at low densities. Purely hadronic stars do not have large masses. For rapid conversions (left panel), there is a hybrid star branch for which the fundamental oscillation frequency verifies $\omega_0^2 > 0$, indicating stability. There is also a small segment of the curve (with dashed lines) which is unstable because $\omega_0^2 < 0$ (this segment also verifies $\partial M/\partial \epsilon_c < 0$). Considering the same equations of state, but assuming that interface conversions are slow (right panel), it is found that the short segment that is unstable in the left panel becomes dynamically stable ($\omega_0^2 > 0$) in spite of having $\partial M/\partial \epsilon_c < 0$.

3.2. Interface Conversions: Slow or Rapid?

As discussed before, the speed of reactions converting hadrons into quarks and vice versa in the neighborhood of a sharp interface at the core of a hybrid star is essential for determining its dynamic stability. Unfortunately, present calculations of the conversion timescale are model dependent. In the following we comment briefly on the predictions of some models.

First, we emphasize that phase transitions are highly collective and nonlinear phenomena, thus, the hadron–quark transition timescale is not expected to be simply the consequence of particles that confine or deconfine independently. Actually, it is known

from a wide variety of systems that the two major mechanisms in which first-order phase transitions proceed are nucleation and spinodal decomposition (see e.g., [81]).

In the case of nucleation, a large conversion timescale is expected due to the existence of a high activation barrier. To understand this argument, we show in Figure 6 a schematic representation of the Gibbs free energy per baryon inside a hybrid star. As already explained in Figure 1, the curves for hadronic matter and quark matter in chemical equilibrium under weak interactions intersect at the pressure p_{tr} . Let us consider a small lump of hadron matter in the neighborhood of the interface, resting in equilibrium at the ‘hadronic side’ of the discontinuity. If the star is unperturbed, this lump is in thermal, mechanical, and chemical equilibrium, like any other fluid element inside the star. In particular, chemical equilibrium under weak interactions determines univocally the particle abundances of all baryon and lepton species at that place. When this small hadronic lump is perturbed radially, it moves to the ‘quark side’ of the interface, which is at a pressure slightly above p_{tr} . At this new position, it is subject to an overpressure that could convert hadrons into quarks if the deconfined quark-matter state had a lower Gibbs free energy per baryon. However, since deconfinement is driven by strong interactions, the quark and lepton abundances Y_i of *just deconfined* quark matter are determined by the composition of the hadronic phase from which the new state emerges; more specifically, by the flavor conservation conditions [30,82–85]:

$$\begin{pmatrix} Y_u \\ Y_d \\ Y_s \end{pmatrix} = \begin{pmatrix} 2 & 1 & 1 & 2 & 1 & 0 & 1 & 0 \\ 1 & 2 & 1 & 0 & 1 & 2 & 0 & 1 \\ 0 & 0 & 1 & 1 & 1 & 1 & 2 & 2 \end{pmatrix} \begin{pmatrix} Y_p \\ Y_n \\ Y_\Lambda \\ Y_{\Sigma^+} \\ Y_{\Sigma^0} \\ Y_{\Sigma^-} \\ Y_{\Xi^0} \\ Y_{\Xi^-} \end{pmatrix}, \tag{5}$$

where $Y_i \equiv n_i/n_B$ is the concentration per baryon of the i -th particle species, and we assume that hadronic matter, in addition to protons and neutrons, may contain some hyperons. Since in general, such condition results in quark matter out of chemical equilibrium against weak interactions, the corresponding state cannot be along the curve Q^{eq} of Figure 6. Calculations show that, if quark matter is to be formed under flavor conservation conditions around the pressure p_{tr} , then its state would be represented by a point 1^* on the curve Q^* , which is always above the point 1^{eq} of phase coexistence in chemical equilibrium (see Figure 6). Since the transition to the point 1^* is energetically suppressed, the perturbed (compressed) hadronic lump will move to the right along the dashed black line of Figure 6. A phase conversion would be possible if the lump is able to reach the point 2^* where the free energy of H^{eq} and Q^* are equal. Therefore, the phase conversion would be rapid if the pressures p_{tr} and p_{tr}^* are close enough to each other and slow if they are sufficiently different. Numerical results using several phenomenological equations of state and different nucleation models [30,84–86] show that the relevant nucleation times are huge, strongly suggesting that the hadron–quark conversion near the interface is slow. A similar reasoning to the one given before holds for the conversion of a quark lump into hadron matter in the vicinity of the interface.

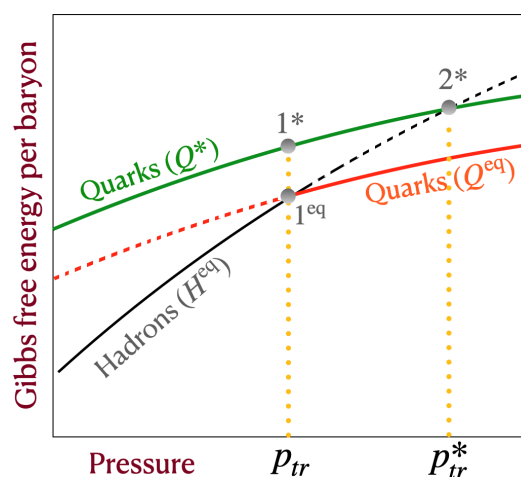


Figure 6. Gibbs free energy per baryon as a function of pressure for catalyzed hadronic matter (curve H^{eq}), catalyzed quark matter (curve Q^{eq}), and quark matter in the 'transition states' (curve Q^*).

In the case of spinodal decomposition, the system must reach the spinodal unstable region after crossing the coexistence frontier. Large enough fluctuations of the density are necessary for this to occur, especially if the density jump between the quark and the hadronic phase is large. Additionally, we must take into account that dissipation mechanisms in quark matter are so strong that they would saturate oscillations at extremely low amplitude. Thus, it is quite possible that the interface oscillates always in the metastable zone, without ever reaching the spinodal region, keeping the over compressed and the over rarefied stellar layers unconverted. In such a case the conversion time would be slow.

Finally, it is worth mentioning that the periodic conversion between quark matter and hadronic matter due to the movement of the interface between them, induced by pressure oscillations in the star, has been analyzed in Reference [87]. In that reference, the analysis suggests that damping grows nonlinearly with the amplitude of the oscillation and that this mechanism is powerful enough to saturate the r -mode at very low saturation amplitude, of order 10^{-10} , being probably the dominant r -mode saturation process in hybrid stars with a sharp interface. The above mechanism should also saturate large amplitude radial oscillations having a strong stabilizing effect on slow-stable hybrid stars.

In summary, there are strong arguments to believe that the conversion timescale would be slow at the interface, although a rapid timescale cannot be discarded.

4. Astrophysical Scenarios for the Formation of Slow Stable Hybrid Stars

In this section we discuss a scenario where the *slow-stable hybrid star* branch can be populated in a realistic astrophysical situation [74]. Many cold hadronic stars in the right panel of Figure 4 are in metastable states because it is energetically convenient for them to convert into more compact *slow-stable hybrid stars* with same baryonic mass. However, these hadronic stars attain p_{tr} only at the center of the maximum mass object. Therefore, mass accretion onto them would not be able to produce *slow-stable hybrid stars*. Indeed, the maximum mass object would collapse into a black hole if further mass were added to it in order to increase the central pressure above p_{tr} . Nonetheless, the situation is different for hot hadronic stars formed in supernovae [88] or in compact star mergers [89,90]. From the QCD phase diagram we expect that the transition density becomes smaller as the temperature increases. Moreover, nucleation models show that the quantum and thermal nucleation timescale of quark matter decreases drastically with temperature (see e.g., Figure 11 of Bombaci et al. [86]). As a consequence, as shown in Figures 14 and 15 of Bombaci et al. [86], the critical stellar mass above which a metastable hadronic star could undergo a phase transition is significantly reduced when the object is hot enough. Notice that, although the critical mass is defined in Bombaci et al. [86], in the context of the coexistence of hadronic stars and strange quark stars, the same reasoning and definitions

can be extended without changes to the case analyzed here. For the equations of state used in Bombaci et al. [86], the critical mass for a proto hadronic star with a typical entropy per baryon $s = 2k_B$ is reduced by $\sim 10\text{--}20\%$ with respect to the value for the cold star. Thus, a significant portion of the upper part of the hadronic branch in the right panel of Figure 4 would be able to decay to the *slow-stable hybrid star* branch in an early evolutionary phase. Hot post-merger hadronic stars would be even more favorable environments for conversion because they can attain temperatures up to 100 MeV [90,91]. Additionally, large density fluctuations are possible in these objects [89,90] which may facilitate the conversion even more. The above scenario does not imply that purely hadronic objects with masses close to the maximum mass cannot exist. Below the ‘hot’ critical mass, a proto-hadronic star would survive the early stages of its evolution without decaying to a *slow-stable hybrid star*. When the hadronic object cools down, the critical mass rises and the star can accrete additional mass from a companion keeping its hadronic nature. This qualitative analysis deserves further investigation, but it suggests that there are feasible astrophysical channels for populating the hadronic and the *slow-stable hybrid star* branch.

5. Implications for Gravitational Wave Astrophysics

Slow-stable hybrid stars tend to have smaller radii than hadronic objects of the same gravitational mass; thus, precise mass and radius measurements could in principle allow their observational differentiation. In addition, future GW detector networks will be able to measure the masses and tidal deformabilities to high accuracy, as well as some quasinormal mode frequencies to within tens of Hz [92]. It has been shown that the tidal deformability of *slow-stable hybrid stars* is significantly smaller [73,74] and the f -mode frequency considerably larger [71] than the corresponding values of hadronic and standard hybrid stars of the same mass. This characteristic is in agreement with claims that hyper-excited dynamical tides, i.e., anomalously small f -mode frequencies, are disfavored by GW170817 [92]. In addition, it is known that discontinuity g -modes can be excited in *slow-stable hybrid stars* but do not exist in the case of rapid conversions due to the absence of a buoyancy force [71]. Moreover, contrary to g -modes of standard hybrid stars which have frequencies below 1 kHz and very long damping times [93], g -modes of *slow-stable hybrid stars* have larger frequencies (1–2 kHz) and much shorter damping times that would make possible their detection by gravitational wave observatories [71].

Since f and g modes are probably the most promising signatures for identifying *slow-stable hybrid stars*, we will give some orders of magnitude of the minimum energy E_{GW} that should be released through them to have detection in present and planned GW observatories. E_{GW} can be estimated from [94,95]:

$$\frac{E_{\text{GW}}}{M_{\odot}c^2} = 3.47 \times 10^{36} \left(\frac{S}{N}\right)^2 \frac{1 + 4Q^2}{4Q^2} \left(\frac{D}{10\text{kpc}}\right)^2 \left(\frac{f}{1\text{kHz}}\right)^2 \left(\frac{S_n}{1\text{Hz}^{-1}}\right), \quad (6)$$

where S/N is the signal-to-noise ratio, $Q = \pi f \tau$ is the quality factor, D the distance to the source, f the frequency, τ the damping time, and S_n the noise power spectral density of the detector. We consider a detector with $S_n^{1/2} \sim 2 \times 10^{-23} \text{ Hz}^{-1/2}$ which is representative of the Advanced LIGO-Virgo at $\sim \text{kHz}$ [9], and another one with $S_n^{1/2} \sim 10^{-24} \text{ Hz}^{-1/2}$ which is illustrative of the planned third-generation ground-based Einstein Observatory at the same frequencies [96]. Taking $S/N = 8$ we calculated the minimum energy E_{GW} that a NS must release through a mode in order to be detected at a distance $D \sim 10 \text{ kpc}$ (star in our Galaxy) and $D \sim 15 \text{ Mpc}$ (star at the Virgo cluster). The results are shown in Table 2. Although it is yet uncertain how much energy will be radiated through the oscillation modes, one can reasonably expect that the energy stored in stellar pulsations is some fraction of the kinetic energy of the formation event. In the case of a typical core collapse supernova, the total released energy is $\sim 10^{53}$ ergs while the kinetic energy of mass ejecta is $\sim 10^{51}$ ergs. Thus, we can expect that some fraction of 10^{51} ergs could be channeled in the f and g pulsation modes of a newly born hybrid star. Notice that, according to Table 2, the g -mode is in some cases easier to detect than the f -mode in spite of having a lower frequency. This is due to

the fact that it has a larger damping time which gives a better quality factor Q . Based on Table 2, we conclude that the observation of f and g modes from an object formed in a core collapse supernova within the Milky Way or in a nearby galaxy looks feasible, since the minimum detectable energy is significantly below $\sim 10^{51}$ ergs for current GW observatories. For binary mergers a detection looks unlikely due to their distances of several Mpc.

Table 2. The minimum estimated energy (in ergs) required in each mode in order to lead to a detection with signal-to-noise ratio of $S/N = 8$ from a pulsating *slow-stable hybrid star* at different distances (local event or at the distance of the Virgo cluster). The results were obtained in Reference [71] using for hadronic matter an EOS based on nuclear interactions derived from chiral effective field theory and for quark matter a generic MIT bag model EOS.

Detector	Distance	f -Mode	g -Mode
LIGO/Virgo	10 kpc	$5 \times 10^{47} - 10^{48}$	$8 \times 10^{46} - 8 \times 10^{47}$
LIGO/Virgo	15 Mpc	$1 - 2 \times 10^{54}$	$2 \times 10^{53} - 2 \times 10^{54}$
Einstein	10 kpc	$1 - 2 \times 10^{45}$	$10^{44} - 10^{45}$
Einstein	15 Mpc	$2 - 5 \times 10^{51}$	$4 \times 10^{50} - 3 \times 10^{51}$

Finally, we will briefly comment about the role of quark/hadron surface tension in binary neutron star merger and core-collapse supernovae simulations. Recently, there has been growing interest in including the possibility of a transition to deconfined quark matter in numerical simulations of these events (see for example [88,90,91,97,98] and references therein). Due to the present lack of knowledge of several aspects of the hadron–quark deconfinement process at high densities, the dynamics of the phase conversion is handled in a very simplified way. For example, no activation barriers for deconfinement are used, equations of state are assumed to be always in chemical equilibrium, and mixed or sharp phases are chosen arbitrarily. Since surface tension plays an important role in nucleation and in the formation of a mixed phase, it would be important that numerical simulations incorporate the results of detailed microscopic calculations of σ .

6. Summary and Conclusions

In this review we have explored some micro-physical properties of the quark–hadron interface in hybrid stars, their consequences for stellar structure and stability, and possible implications for gravitational wave astrophysics. Microscopic calculations of the surface tension span a wide range of values depending the equations of state and the method used for the calculation, which makes it uncertain whether the quark–hadron interface is mixed or sharp. However, recent results show that repulsive vector interactions strongly increase the quark matter surface tension [47], giving support to the scenario of a sharp separation between both phases. We have also discussed the role of the conversion speed between hadronic and quark matter at the interface, when the star is dynamically perturbed. If phase conversions have a slower timescale that the perturbation period (typically around 1 millisecond), a new class of dynamically stable hybrid objects is possible. Huge densities (tens of times larger than the nuclear saturation density) can be attained at the center of these stars. These objects could be produced during the proton-neutron star phase after a core collapse supernova explosion or in the aftermath of a binary compact star merger. Discontinuity gravity oscillation modes are the most clear signature for their observational identification.

Author Contributions: All authors discussed the results and contributed to the final manuscript. All authors have read and agreed to the published version of the manuscript.

Funding: G. Lugones was supported in part by CNPq-Brazil (grant 309767/2017-2) and FAPESP-Brazil (grant 2013/10559-5). A. G. Grunfeld was supported by CONICET-Argentina (grant PIP17-700).

Institutional Review Board Statement: Not applicable.

Informed Consent Statement: Not applicable.

Conflicts of Interest: The authors declare no conflict of interest.

References

- Demorest, P.; Pennucci, T.; Ransom, S.; Roberts, M.; Hessels, J. Shapiro Delay Measurement of A Two Solar Mass Neutron Star. *Nature* **2010**, *467*, 1081–1083. [[CrossRef](#)]
- Antoniadis, J.; Freire, P.C.; Wex, N.; Tauris, T.M.; Lynch, R.S.; Van Kerkwijk, M.H.; Kramer, M.; Bassa, C.; Dhillon, V.S.; Driebe, T.; et al. A Massive Pulsar in a Compact Relativistic Binary. *Science* **2013**, *340*, 6131. [[CrossRef](#)] [[PubMed](#)]
- Cromartie, H.T.; Fonseca, E.; Ransom, S.M.; Demorest, P.B.; Arzoumanian, Z.; Blumer, H.; Brook, P.R.; DeCesar, M.E.; Dolch, T.; Ellis, J.A.; et al. Relativistic Shapiro delay measurements of an extremely massive millisecond pulsar. *Nat. Astron.* **2019**, *4*, 72–76. [[CrossRef](#)]
- Linares, M.; Shahbaz, T.; Casares, J. Peering into the dark side: Magnesium lines establish a massive neutron star in PSR J2215+5135. *Astrophys. J.* **2018**, *859*, 54. [[CrossRef](#)]
- Riley, T.E.; Watts, A.L.; Bogdanov, S.; Ray, P.S.; Ludlam, R.M.; Guillot, S.; Arzoumanian, Z.; Baker, C.L.; Bilous, A.V.; Chakrabarty, D.; et al. A NICER View of PSR J0030+0451: Millisecond Pulsar Parameter Estimation. *Astrophys. J. Lett.* **2019**, *887*, L21. [[CrossRef](#)]
- Miller, M.C.; Lamb, F.K.; Dittmann, A.J.; Bogdanov, S.; Arzoumanian, Z.; Gendreau, K.C.; Guillot, S.; Harding, A.K.; Ho, W.C.G.; Lattimer, J.M. PSR J0030+0451 Mass and Radius from NICER Data and Implications for the Properties of Neutron Star Matter. *Astrophys. J. Lett.* **2019**, *887*, L24. [[CrossRef](#)]
- Riley, T.E.; Watts, A.L.; Ray, P.S.; Bogdanov, S.; Guillot, S.; Morsink, S.M.; Bilous, A.V.; Arzoumanian, Z.; Choudhury, D.; Deneva, J.S.; et al. A NICER View of the Massive Pulsar PSR J0740+6620 Informed by Radio Timing and XMM-Newton Spectroscopy. *Astrophys. J. Lett.* **2021**, *918*, L27. [[CrossRef](#)]
- Miller, M.C.; Lamb, F.K.; Dittmann, A.J.; Bogdanov, S.; Arzoumanian, Z.; Gendreau, K.C.; Guillot, S.; Ho, W.C.; Lattimer, J.M.; Loewenstein, M.; et al. The Radius of PSR J0740+6620 from NICER and XMM-Newton Data. *APJ Lett.* **2021**, Submitted. [[CrossRef](#)]
- Abbott, B.P.; Abbott, R.; Abbott, T.D.; Acernese, F.; Ackley, K.; Adams, C.; Adams, T.; Addesso, P.; Adhikari, R.X.; Adya, V.B.; et al. GW170817: Observation of Gravitational Waves from a Binary Neutron Star Inspiral. *Phys. Rev. Lett.* **2017**, *119*, 161101 [[CrossRef](#)]
- Annala, E.; Gorda, T.; Kurkela, A.; Vuorinen, A. Gravitational-wave constraints on the neutron-star-matter Equation of State. *Phys. Rev. Lett.* **2018**, *120*, 172703. [[CrossRef](#)]
- Most, E.R.; Weih, L.R.; Rezzolla, L.; Schaffner-Bielich, J. New constraints on radii and tidal deformabilities of neutron stars from GW170817. *Phys. Rev. Lett.* **2018**, *120*, 261103. [[CrossRef](#)]
- Raithel, C.; Özel, F.; Psaltis, D. Tidal deformability from GW170817 as a direct probe of the neutron star radius. *Astrophys. J. Lett.* **2018**, *857*, L23. [[CrossRef](#)]
- Capano, C.D.; Tews, I.; Brown, S.M.; Margalit, B.; De, S.; Kumar, S.; Brown, D.A.; Krishnan, B.; Reddy, S. Stringent constraints on neutron-star radii from multimessenger observations and nuclear theory. *Nat. Astron.* **2020**, *4*, 625–632. [[CrossRef](#)]
- Abbott, B.P.; Abbott, R.; Abbott, T.D.; Acernese, F.; Ackley, K.; Adams, C.; Adams, T.; Addesso, P.; Adhikari, R.X.; Adya, V.B.; et al. GW170817: Measurements of neutron star radii and equation of state. *Phys. Rev. Lett.* **2018**, *121*, 161101. [[CrossRef](#)]
- Rezzolla, L.; Most, E.R.; Weih, L.R. Using Gravitational-wave Observations and Quasi-universal Relations to Constrain the Maximum Mass of Neutron Stars. *Astrophys. J.* **2018**, *852*, L25. [[CrossRef](#)]
- Abbott, B.P.; Abbott, R.; Abbott, T.D.; Abraham, S.; Acernese, F.; Ackley, K.; Adams, C.; Adhikari, R.X.; Adya, V.B.; Affeldt, C.; et al. GW190425: Observation of a Compact Binary Coalescence with Total Mass $\sim 3.4M_{\odot}$. *Astrophys. J. Lett.* **2020**, *892*, L3. [[CrossRef](#)]
- Han, M.Z.; Tang, S.P.; Hu, Y.M.; Li, Y.J.; Jiang, J.L.; Jin, Z.P.; Fan, Y.Z.; Wei, D.M. Is GW190425 consistent with being a neutron star–black hole merger? *Astrophys. J. Lett.* **2020**, *891*, L5. [[CrossRef](#)]
- Kyutoku, K.; Fujibayashi, S.; Hayashi, K.; Kawaguchi, K.; Kiuchi, K.; Shibata, M.; Tanaka, M. On the Possibility of GW190425 Being a Black Hole–Neutron Star Binary Merger. *Astrophys. J. Lett.* **2020**, *890*, L4. [[CrossRef](#)]
- Abbott, R.; Abbott, T.D.; Abraham, S.; Acernese, F.; Ackley, K.; Adams, C.; Adhikari, R.X.; Adya, V.B.; Affeldt, C.; Agathos, M.; et al. GW190814: Gravitational Waves from the Coalescence of a 23 Solar Mass Black Hole with a 2.6 Solar Mass Compact Object. *Astrophys. J. Lett.* **2020**, *896*, L44. [[CrossRef](#)]
- Ayriyan, A.; Blaschke, D.; Grunfeld, A.G.; Alvarez-Castillo, D.; Grigorian, H.; Abgaryan, V. Bayesian analysis of multimessenger M-R data with interpolated hybrid EoS. *arXiv* **2021**, arXiv:2102.13485.
- Dexheimer, V.; Gomes, R.O.; Klähn, T.; Han, S.; Salinas, M. GW190814 as a massive rapidly rotating neutron star with exotic degrees of freedom. *Phys. Rev. C* **2021**, *103*, 025808. [[CrossRef](#)]
- Bombaci, I.; Drago, A.; Logoteta, D.; Pagliara, G.; Vidaña, I. Was GW190814 a Black Hole–Strange Quark Star System? *Phys. Rev. Lett.* **2021**, *126*, 162702. [[CrossRef](#)] [[PubMed](#)]
- Abbott, R.; Abbott, T.D.; Abraham, S.; Acernese, F.; Ackley, K.; Adams, A.; Adams, C.; Adhikari, R.X.; Adya, V.B.; Affeldt, C.; et al. Observation of Gravitational Waves from Two Neutron Star–Black Hole Coalescences. *Astrophys. J. Lett.* **2021**, *915*, L5. [[CrossRef](#)]
- Abbott, R.; Abbott, T.D.; Acernese, F.; Ackley, K.; Adams, C.; Adhikari, N.; Adhikari, R.X.; Adya, V.B.; Affeldt, C.; Agarwal, D.; et al. GWTC-3: Compact Binary Coalescences Observed by LIGO and Virgo During the Second Part of the Third Observing Run. *arXiv* **2021**, arXiv:2111.03606.

25. Buballa, M.; Carignano, S. Self-bound quark matter in the NJL model revisited: From schematic droplets to domain-wall solitons. *Phys. Rev. D* **2013**, *87*, 054004. [[CrossRef](#)]
26. Pinto, M.B.; Koch, V.; Randrup, J. The Surface Tension of Quark Matter in a Geometrical Approach. *Phys. Rev. C* **2012**, *86*, 025203. [[CrossRef](#)]
27. Wen, X.J.; Li, J.Y.; Liang, J.Q.; Peng, G.X. Medium effects on the surface tension of strangelets in the extended quasiparticle model. *Phys. Rev. C* **2010**, *82*, 025809. [[CrossRef](#)]
28. Palhares, L.F.; Fraga, E.S. Droplets in the cold and dense linear sigma model with quarks. *Phys. Rev. D* **2010**, *82*, 125018. [[CrossRef](#)]
29. Carmo, T.A.S.d.; Lugones, G.; Grunfeld, A.G. Nucleation rate of color superconducting droplets in protoneutron stars. *J. Phys. G* **2013**, *40*, 035201. [[CrossRef](#)]
30. Lugones, G.; Grunfeld, A.G. Critical spectrum of fluctuations for deconfinement at proto-neutron star cores. *Phys. Rev. D* **2011**, *84*, 085003. [[CrossRef](#)]
31. Jaikumar, P.; Reddy, S.; Steiner, A.W. The Strange star surface: A Crust with nuggets. *Phys. Rev. Lett.* **2006**, *96*, 041101. [[CrossRef](#)]
32. Alford, M.G.; Rajagopal, K.; Reddy, S.; Steiner, A.W. The Stability of strange star crusts and strangelets. *Phys. Rev. D* **2006**, *73*, 114016. [[CrossRef](#)]
33. Lugones, G.; Grunfeld, A.G. Surface and curvature properties of charged strangelets in compact objects. *Phys. Rev. C* **2021**, *103*, 035813. [[CrossRef](#)]
34. Voskresensky, D.N.; Yasuhira, M.; Tatsumi, T. Charge screening at first order phase transitions and hadron quark mixed phase. *Nucl. Phys. A* **2003**, *723*, 291–339. [[CrossRef](#)]
35. Tatsumi, T.; Yasuhira, M.; Voskresensky, D.N. Hadron quark mixed phase in neutron stars. *Nucl. Phys. A* **2003**, *718*, 359–362. [[CrossRef](#)]
36. Maruyama, T.; Chiba, S.; Schulze, H.J.; Tatsumi, T. Hadron-quark mixed phase in hyperon stars. *Phys. Rev. D* **2007**, *76*, 123015. [[CrossRef](#)]
37. Endo, T. Region of hadron-quark mixed phase in hybrid stars. *Phys. Rev. C* **2011**, *83*, 068801. [[CrossRef](#)]
38. Maslov, K.; Yasutake, N.; Ayriyan, A.; Blaschke, D.; Grigorian, H.; Maruyama, T.; Tatsumi, T.; Voskresensky, D.N. Hybrid equation of state with pasta phases and third family of compact stars. *Phys. Rev.* **2019**, *C100*, 025802. [[CrossRef](#)]
39. Xia, C.J.; Maruyama, T.; Yasutake, N.; Tatsumi, T. Constraining quark-hadron interface tension in the multimessenger era. *Phys. Rev. D* **2019**, *99*, 103017. [[CrossRef](#)]
40. Ju, M.; Wu, X.; Ji, F.; Hu, J.; Shen, H. Hadron-quark mixed phase in the quark-meson coupling model. *Phys. Rev. C* **2021**, *103*, 025809. [[CrossRef](#)]
41. Yasutake, N.; Lastowiecki, R.; Benic, S.; Blaschke, D.; Maruyama, T.; Tatsumi, T. Finite-size effects at the hadron-quark transition and heavy hybrid stars. *Phys. Rev. C* **2014**, *89*, 065803. [[CrossRef](#)]
42. Wu, X.; Shen, H. Finite-size effects on the hadron-quark phase transition in neutron stars. *Phys. Rev. C* **2017**, *96*, 025802. [[CrossRef](#)]
43. Wu, X.; Shen, H. Nuclear symmetry energy and hadron-quark mixed phase in neutron stars. *Phys. Rev. C* **2019**, *99*, 065802. [[CrossRef](#)]
44. Xia, C.J.; Maruyama, T.; Yasutake, N.; Tatsumi, T.; Shen, H.; Togashi, H. Systematic study on the quark-hadron mixed phase in compact stars. *Phys. Rev.* **2020**, *D102*, 023031. [[CrossRef](#)]
45. Balian, R.; Bloch, C. Distribution of eigenfrequencies for the wave equation in a finite domain. 1. Three-dimensional problem with smooth boundary surface. *Ann. Phys.* **1970**, *60*, 401–447. [[CrossRef](#)]
46. Hansson, T.H.; Jaffe, R.L. The Multiple Reflection Expansion for Confined Scalar, Dirac and Gauge Fields. *Ann. Phys.* **1983**, *151*, 204. [[CrossRef](#)]
47. Lugones, G.; Grunfeld, A.G. Vector interactions inhibit quark-hadron mixed phases in neutron stars. *Phys. Rev. D* **2021**, *104*, L101301. [[CrossRef](#)]
48. Shchepochin, N.N.; Chugunov, A.I. Surface energy of nuclear matter above and below neutron drip with the Skyrme-type effective interactions. *J. Phys. Conf. Ser.* **2020**, *1697*, 012025. [[CrossRef](#)]
49. Douchin, F.; Haensel, P.; Meyer, J. Nuclear surface and curvature properties for SLy Skyrme forces and nuclei in the inner neutron-star crust. *Nucl. Phys. A* **2000**, *665*, 419–446. [[CrossRef](#)]
50. Avancini, S.S.; Menezes, D.P.; Alloy, M.D.; Marinelli, J.R.; Moraes, M.M.W.; Providencia, C. Warm and cold pasta phase in relativistic mean field theory. *Phys. Rev. C* **2008**, *78*, 015802. [[CrossRef](#)]
51. Huang, S.; Potvin, J.; Rebbi, C.; Sanielevici, S. Surface Tension in Finite Temperature Quantum Chromodynamics. *Phys. Rev. D* **1990**, *42*, 2864; Erratum in *Phys. Rev. D* **1991**, *43*, 2056. [[CrossRef](#)] [[PubMed](#)]
52. Alves, N.A. Surface tension in SU(3) at finite temperature. *Phys. Rev. D* **1992**, *46*, 3678–3681. [[CrossRef](#)]
53. Kajantie, K.; Karkkainen, L.; Rummukainen, K. Tension of the interface between two ordered phases in lattice SU(3) gauge theory. *Nucl. Phys. B* **1991**, *357*, 693–712. [[CrossRef](#)]
54. Brower, R.; Huang, S.; Potvin, J.; Rebbi, C. The Surface tension of nucleating hadrons using the free energy of an isolated quark. *Phys. Rev. D* **1992**, *46*, 2703–2708. [[CrossRef](#)]
55. Berger, M.; Jaffe, R. Radioactivity in strange quark matter. *Phys. Rev. C* **1987**, *35*, 213–225. [[CrossRef](#)]
56. Lugones, G.; Grunfeld, A.G. Surface tension of highly magnetized degenerate quark matter. *Phys. Rev. C* **2017**, *95*, 015804. [[CrossRef](#)]

57. Lugones, G.; Grunfeld, A.G. Surface tension of hot and dense quark matter under strong magnetic fields. *Phys. Rev. C* **2019**, *C99*, 035804. [[CrossRef](#)]
58. Garcia, A.F.; Pinto, M.B. Surface tension of magnetized quark matter. *Phys. Rev. C* **2013**, *88*, 025207. [[CrossRef](#)]
59. Ke, W.Y.; Liu, Y.X. Interface tension and interface entropy in the 2+1 flavor Nambu-Jona-Lasinio model. *Phys. Rev. D* **2014**, *89*, 074041. [[CrossRef](#)]
60. Kroff, D.; Fraga, E.S. Nucleating quark droplets in the core of magnetars. *Phys. Rev. D* **2015**, *91*, 025017. [[CrossRef](#)]
61. Mintz, B.W.; Stiele, R.; Ramos, R.O.; Schaffner-Bielich, J. Phase diagram and surface tension in the three-flavor Polyakov-quark-meson model. *Phys. Rev. D* **2013**, *87*, 036004. [[CrossRef](#)]
62. Gao, F.; Liu, Y.X. Interface Effect in QCD Phase Transitions via Dyson-Schwinger Equation Approach. *Phys. Rev. D* **2016**, *94*, 094030. [[CrossRef](#)]
63. Fraga, E.S.; Hippert, M.; Schmitt, A. Surface tension of dense matter at the chiral phase transition. *Phys. Rev. D* **2019**, *D99*, 014046. [[CrossRef](#)]
64. Xia, C.J.; Peng, G.X.; Sun, T.T.; Guo, W.L.; Lu, D.H.; Jaikumar, P. Interface effects of strange quark matter with density dependent quark masses. *Phys. Rev. D* **2018**, *98*, 034031. [[CrossRef](#)]
65. Lugones, G.; Grunfeld, A.; Al Ajmi, M. Surface tension and curvature energy of quark matter in the Nambu-Jona-Lasinio model. *Phys. Rev. C* **2013**, *88*, 045803. [[CrossRef](#)]
66. Chandrasekhar, S. The Dynamical Instability of Gaseous Masses Approaching the Schwarzschild Limit in General Relativity. *Astrophys. J.* **1964**, *140*, 417–433; Erratum in *Astrophys. J.* **1964**, *140*, 1342. [[CrossRef](#)]
67. Harrison, B.; Thorne, K.; Wakano, M.; Wheeler, J. *Gravitation Theory and Gravitational Collapse*; University of Chicago Press: Chicago, IL, USA, 1965.
68. Vasquez Flores, C.; Lenzi, C.; Lugones, G. Radial pulsations of hybrid neutron stars. *Int. J. Mod. Phys. Conf. Ser.* **2012**, *18*, 105–108. [[CrossRef](#)]
69. Pereira, J.P.; Flores, C.V.; Lugones, G. Phase transition effects on the dynamical stability of hybrid neutron stars. *Astrophys. J.* **2018**, *860*, 12. [[CrossRef](#)]
70. Mariani, M.; Orsaria, M.G.; Ranea-Sandoval, I.F.; Lugones, G. Magnetized hybrid stars: Effects of slow and rapid phase transitions at the quark-hadron interface. *Mon. Not. R. Astron. Soc.* **2019**, *489*, 4261–4277. [[CrossRef](#)]
71. Tonetto, L.; Lugones, G. Discontinuity gravity modes in hybrid stars: Assessing the role of rapid and slow phase conversions. *Phys. Rev. D* **2020**, *101*, 123029. [[CrossRef](#)]
72. Pereira, J.P.; Bejger, M.; Tonetto, L.; Lugones, G.; Haensel, P.; Zdunik, J.L.; Sieniawska, M. Probing elastic quark phases in hybrid stars with radius measurements. *Astrophys. J.* **2021**, *910*, 145. [[CrossRef](#)]
73. Parisi, A.; Flores, C.V.; Lenzi, C.H.; Chen, C.S.; Lugones, G. Hybrid stars in the light of the merging event GW170817. *J. Cosmol. Astropart. Phys.* **2021**, *2021*, 42. [[CrossRef](#)]
74. Lugones, G.; Mariani, M.; Ranea-Sandoval, I.F. Slow stable hybrid stars: A new class of compact stars that fulfills all current observational constraints. **2021**, Submitted.
75. Flores, C.V.; Castro, L.B.; Lugones, G. Properties of strongly magnetized ultradense matter and its effects on magnetar pulsations. *Phys. Rev. C* **2016**, *94*, 015807. [[CrossRef](#)]
76. Vasquez Flores, C.; Lugones, G. Radial oscillations of color superconducting self-bound quark stars. *Phys. Rev. D* **2010**, *82*, 063006. [[CrossRef](#)]
77. Benvenuto, O.G.; Lugones, G. The properties of strange stars in the quark mass-density-dependent model. *Int. J. Mod. Phys. D* **1998**, *7*, 29–48. [[CrossRef](#)]
78. Jiménez, J.C.; Fraga, E.S. Radial oscillations in neutron stars from QCD. *Phys. Rev. D* **2021**, *104*, 014002. [[CrossRef](#)]
79. Gondek, D.; Haensel, P.; Zdunik, J.L. Radial pulsations and stability of proton-neutron stars. *Astron. Astrophys.* **1997**, *325*, 217–227.
80. Di Clemente, F.; Mannarelli, M.; Tonelli, F. Reliable description of the radial oscillations of compact stars. *Phys. Rev. D* **2020**, *101*, 103003. [[CrossRef](#)]
81. Slezov, V.V. *Kinetics of First-Order Phase Transitions*; John Wiley & Sons, Ltd.: Hoboken, NJ, USA, 2009. ISBN 978-3-527-62777-6. [[CrossRef](#)]
82. Olesen, M.L.; Madsen, J. Nucleation of quark matter bubbles in neutron stars. *Phys. Rev. D* **1994**, *49*, 2698–2702. [[CrossRef](#)] [[PubMed](#)]
83. Lugones, G.; Benvenuto, O. Effect of trapped neutrinos in the hadron matter to quark matter transition. *Phys. Rev. D* **1998**, *58*, 083001. [[CrossRef](#)]
84. Iida, K.; Sato, K. Effects of hyperons on the dynamical deconfinement transition in cold neutron star matter. *Phys. Rev. C* **1998**, *58*, 2538–2559. [[CrossRef](#)]
85. Bombaci, I.; Parenti, I.; Vidana, I. Quark deconfinement and implications for the radius and the limiting mass of compact stars. *Astrophys. J.* **2004**, *614*, 314–325. [[CrossRef](#)]
86. Bombaci, I.; Logoteta, D.; Vidaña, I.; Providência, C. Quark matter nucleation in neutron stars and astrophysical implications. *Eur. Phys. J. A* **2016**, *52*, 58. [[CrossRef](#)]
87. Alford, M.G.; Han, S.; Schwenzer, K. Phase conversion dissipation in multicomponent compact stars. *Phys. Rev. C* **2015**, *91*, 055804. [[CrossRef](#)]

88. Fischer, T.; Bastian, N.U.F.; Wu, M.R.; Baklanov, P.; Sorokina, E.; Blinnikov, S.; Typel, S.; Klähn, T.; Blaschke, D.B. Quark deconfinement as a supernova explosion engine for massive blue supergiant stars. *Nat. Astron.* **2018**, *2*, 980–986. [[CrossRef](#)]
89. Baiotti, L.; Giacomazzo, B.; Rezzolla, L. Accurate evolutions of inspiralling neutron-star binaries: Prompt and delayed collapse to black hole. *Phys. Rev. D* **2008**, *78*, 084033. [[CrossRef](#)]
90. Weih, L.R.; Hanauske, M.; Rezzolla, L. Postmerger Gravitational-Wave Signatures of Phase Transitions in Binary Mergers. *Phys. Rev. Lett.* **2020**, *124*, 171103. [[CrossRef](#)]
91. Bauswein, A.; Bastian, N.U.F.; Blaschke, D.B.; Chatziioannou, K.; Clark, J.A.; Fischer, T.; Oertel, M. Identifying a first-order phase transition in neutron star mergers through gravitational waves. *Phys. Rev. Lett.* **2019**, *122*, 061102. [[CrossRef](#)]
92. Pratten, G.; Schmidt, P.; Hinderer, T. Gravitational-Wave Asteroseismology with Fundamental Modes from Compact Binary Inspirals. *Nat. Commun.* **2020**, *11*, 2553. [[CrossRef](#)] [[PubMed](#)]
93. Miniutti, G.; Pons, J.A.; Berti, E.; Gualtieri, L.; Ferrari, V. Non-radial oscillation modes as a probe of density discontinuities in neutron stars. *Mon. Not. R. Astron. Soc.* **2003**, *338*, 389–400. [[CrossRef](#)]
94. Andersson, N.; Ferrari, V.; Jones, D.I.; Kokkotas, K.D.; Krishnan, B.; Read, J.S.; Rezzolla, L.; Zink, B. Gravitational waves from neutron stars: Promises and challenges. *Gen. Relativ. Gravit.* **2011**, *43*, 409–436. [[CrossRef](#)]
95. Kokkotas, K.D.; Apostolatos, T.A.; Andersson, N. The inverse problem for pulsating neutron stars: A ‘fingerprint analysis’ for the supranuclear equation of state. *Mon. Not. R. Astron. Soc.* **2001**, *320*, 307–315. [[CrossRef](#)]
96. Abbott, B.P.; Abbott, R.; Abbott, T.D.; Abernathy, M.R.; Ackley, K.; Adams, C.; Addesso, P.; Adhikari, R.X.; Adya, V.B.; Affeldt, C.; et al. Exploring the sensitivity of next generation gravitational wave detectors. *Class. Quantum Gravity* **2017**, *34*, 044001. [[CrossRef](#)]
97. Kashyap, R.; Das, A.; Radice, D.; Padamata, S.; Prakash, A.; Logoteta, D.; Perego, A.; Godzieba, D.A.; Bernuzzi, S.; Bombaci, I.; et al. Numerical relativity simulations of prompt collapse mergers: Threshold mass and phenomenological constraints on neutron star properties after GW170817. *arXiv* **2021**, arXiv:2111.05183.
98. Prakash, A.; Radice, D.; Logoteta, D.; Perego, A.; Nedora, V.; Bombaci, I.; Kashyap, R.; Bernuzzi, S.; Endrizzi, A. Signatures of deconfined quark phases in binary neutron star mergers. *Phys. Rev. D* **2021**, *104*, 083029. [[CrossRef](#)]